Engineering with Computers (2021) 37:3359–3374
https://doi.org/10.1007/s00366-020-01002-1

ORIGINAL ARTICLE

Application of nonlocal strain–stress gradient theory and GDQEM for thermo-vibration responses of a laminated composite nanoshell

Hossein Moayedi[1,2] · Farzad Ebrahimi[3] · Mostafa Habibi[4,5] · Hamed Safarpour[3] · Loke Kok Foong[6,7]

Received: 7 February 2020 / Accepted: 2 March 2020 / Published online: 14 March 2020

Abstract
In this article, thermal buckling and frequency analysis of a size-dependent laminated composite cylindrical nanoshell in thermal environment using nonlocal strain–stress gradient theory are presented. The thermodynamic equations of the laminated cylindrical nanoshell are based on first-order shear deformation theory, and generalized differential quadrature element method is implemented to solve these equations and obtain natural frequency and critical temperature of the presented model. The results show that by considering C–F boundary conditions and every even layers' number, in lower value of length scale parameter, by increasing the length scale parameter, the frequency of the structure decreases but in higher value of length scale parameter this matter is inverse. Finally, influences of temperature difference, ply angle, length scale and nonlocal parameters on the critical temperature and frequency of the laminated composite nanostructure are investigated.

Keywords Laminated nanoshell · Hamilton's principle · NSGT · GDQEM · Frequency response

1 Introduction

Owing to the recent advancement in mechanical and material sciences [1–3], FG and laminated composites have attracted in plenty of applications [4–14]. Many researches show that [15–19] the laminated composite structures have a better dynamic response in comparison with the isotropic and other materials. Safarpour et al. [20] modeled a laminated nanoshell in a thermal environment and investigated the wave dispersion of the structure. They analyzed the size effects with the aid of NSGT. They found that it is not accepted which by increasing the number of layers of the laminated structure the dynamic stability improves. They reported that the number of layers has an optimum number. Zeighampour et al. [21] presented a mathematical modeling for investigation of wave dispersion of the laminated nanoshell MSGT and thin theory. They claimed that MSGT encounter us with accurate result in comparison with classical theory. Sahmani et al. [22] presented the dynamic and static response of the laminated beams which are reinforced with GPLs. They modeled the structure with the aid of NSGT. They found that initial load decreases the frequency

✉ Farzad Ebrahimi
febrahimy@gmail.com

✉ Loke Kok Foong
lokekokfoong@duytan.edu.vn

Hossein Moayedi
hossein.moayedi@tdtu.edu.vn

Mostafa Habibi
Habibi_mech@yahoo.com

Hamed Safarpour
Hamed_safarpor@yahoo.com

1 Informetrics Research Group, Ton Duc Thang University, Ho Chi Minh City, Vietnam

2 Faculty of Civil Engineering, Ton Duc Thang University, Ho Chi Minh City, Vietnam

3 Mechanical Engineering Department, Faculty of Engineering, Imam Khomeini International University, Qazvin, Iran

4 Center of Excellence in Design, Robotics and Automation. School of Mechanical Engineering, Sharif University of Technology, Tehran, Iran

5 Department of Mechanical Engineering, Sharif University of Technology, Tehran, Iran

6 Institute of Research and Development, Duy Tan University, Da Nang 550000, Vietnam

7 Faculty of Civil Engineering, Duy Tan University, Da Nang 550000, Vietnam

of the structure. Nonlocal effects on the dynamic and static responses of the micro-/nanostructure are presented in Refs [23–29].

In the scope of dynamic behavior of the piezoelectric cylindrical shell [30–32], Shojaeefard et al. [33] dealt with frequency analysis for different boundary conditions on a rotary cylindrical piezoelectric nanoshell surrounded by an elastic foundation. Also, they used GDQ method for solving the problems. Dehkordi et al. [34] studied vibrational behavior of a piezoelectric conic nanotube using moderately thin model and a size-dependent theory. They investigated the effects of flex electric on the frequency of the nanosmart tube. Arefi [35] employed nonlocal elasticity theory and FSDT for investigation of bending behavior of a doubly curved piezoelectric nanoshell. The nanostructure is exposed to transverse loads, voltage and surrounded with Winkler–Pasternak foundation. They in this work examined the effects of nonlocal parameter, applied voltage, viscoelastic parameters on the electromechanic behaviors of the piezonanostructure. Razavi et al. [36] modeled a piezoelectric nanoshell which is composed with functionally graded (FG) and piezoelectric materials. They presented influences of dimensional parameters on the frequency behavior of the piezoelectric nanostructures. Ninh and Bich [37] demonstrated the nonlinear dynamic behavior of the electrically FG nanocylindrical shells in the thermal conditions. A FG shell reinforced with carbon nanotube is modeled in a condition that outer and inner surfaces were surrounded by piezolayers. Fangand et al. [38] engaged with thick theory and electromechanic theory for investigation of nonlinear frequency of a nanoshell surrounded by a piezolayer. They studied the amplitude frequency curves of the nanoshell. Eftekhari et al. [39] investigated vibrational property of a FG cylindrical shell reinforced with carbon nanotube and the structure surrounded by PIAC in an orthotropic elastic medium and thermal site. They in this work employed an analytical method and DQ method in other to figure out the equations, and they presented influences of electromagnetic field and various patterns of CNT ratio on dynamic behaviors of the system. Vinyas [40] encountered with FE modeling for frequency analysis of a plate which this structure has an MEE property. He considered moderately thick theory for modeling the problem. He emphasized that CNT pattern and volume of the reinforcement have a significant impact on the free vibration of the structure. Zhu et al. [41] did a study on the free vibration of a PIAC nanocylindrical shell, and by employing the perturbation method, they solved the governing equations. They investigated the impact of surface energy on the dynamic behaviors of the nanosmart structure. Singh et al. [42] with the aid of a numerically method modeled curved panel. The structure covered with the PIAC. Their results showed the effect of piezolayer on the frequency of the nanostructure. Fan et al. [43] conducted research into free vibration of a conical nanostructure. Inner and outer layers of a conical CNTRC are surrounded by piezolayers. In the field of critical temperature of the cylindrical shell structures, Refs [20, 44] presented thermal static and dynamic behaviors of FG shells beneath some geometrical imperfection and various load conditions. Their results demonstrate that the behavior of the cylindrical structure beneath the nonlinear change of temperature is more stable in comparison with a linear change in temperature through thickness. Vibration, buckling, wave propagation and bending responses of the nanocomposite-reinforced structures are investigated in Refs [45–60].

Also, Wang et al. [61] carried out research into critical thermal loading for a shell based on a theoretical method. The main conclusion of the paper reported a theoretical method for finding the critical temperature of that structure. Safarpour et al. [62] presented an exact numerical method for investigation buckling, free and forced vibration of a FG nanoshell in a thermal site. Some theories with consideration thickness stretching effect are employed in Refs [63–70] for investigation vibrational behavior of the composite structures. In the field of stability analysis of the structures, Safarpour et al. [30, 33, 71–82] presented buckling and vibrational analysis of the structures with various geometrical parameters.

For the first time, the presented study investigates the thermodynamic analysis of a laminated composite cylindrical nanoshell based on NSGT considering the exact values of nonlocal constants and material length scale parameters. The thermodynamic equations of the laminated cylindrical nanoshell are based on FSDT, and GDQEM is implemented to solve these equations and obtain natural frequency and critical temperature of the current model. Finally, using mentioned continuum mechanics theory, the investigation has been made into the influence of the temperature difference and the different types of the laminated composites on the critical temperature difference and dynamic stability of the laminated composite nanostructure.

2 Theory and formulation

In Fig. 1, a laminated composite nanoshell with consideration of thermal effects is sketched, where R is the radius of tube's middle surface and h is the thickness of the nanoshell. Also, $\bar{\theta}$ is the ply angle of each layer. The material of the nanostructure is considered as a laminated composite.

2.1 NSG model

The fundamental equation can be expressed as follows due to the NSG model [83]:

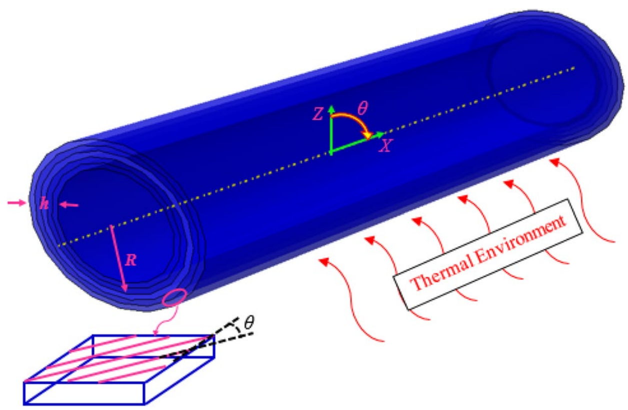

Fig. 1 The geometry of a laminated composite nanoshell

$$(1-\mu^2\nabla^2)t_{ij} = C_{ijck}(1-l^2\nabla^2)\varepsilon_{ck} \tag{1}$$

where $\nabla^2 = \partial^2/\partial x^2 + \partial^2/R^2\partial\theta^2$; t_{ij}, C_{ijck} and ε_{ck}, respectively, are the NSG stress, elasticity tensors and strain. The tensor of NSG stress can be defined as follows [83]:

$$t_{ij} = \sigma_{ij} - \nabla\sigma_{ij}^{(1)} \tag{2}$$

where σ_{ij} and $\sigma_{ij}^{(1)}$ presented the components of basic and nanosize stresses, respectively. The l and μ are constant values standing for the higher-order strain gradient stress and noninvariant influence. Recent experimental researches also demonstrated the calibrated values of the size-dependent factors. The strain tensor could be written as:

$$\varepsilon_{ij} = \frac{1}{2}\left(u_{i,j} + u_{j,i}\right) \tag{3}$$

where u_i stands for the elements of the displacement vector. Due to Eq (2), the relation between stress and strain of the mentioned structure would be presented as [84]:

$$\begin{bmatrix} t_{xx} \\ t_{\theta\theta} \\ t_{x\theta} \end{bmatrix} = \frac{(1-l^2\nabla^2)}{(1-\mu^2\nabla^2)} \begin{bmatrix} C_{11} & C_{12} & 0 \\ C_{12} & C_{22} & 0 \\ 0 & 0 & C_{66} \end{bmatrix}^{(L)} \begin{bmatrix} \varepsilon_{xx} - \alpha\Delta T \\ \varepsilon_{\theta\theta} - \alpha\Delta T \\ \varepsilon_{x\theta} \end{bmatrix},$$
$$\begin{bmatrix} t_{\theta z} \\ t_{xz} \end{bmatrix} = \frac{(1-l^2\nabla^2)}{(1-\mu^2\nabla^2)} \begin{bmatrix} C_{44} & 0 \\ 0 & C_{55} \end{bmatrix}^{(L)} \begin{bmatrix} \varepsilon_{\theta z} \\ \varepsilon_{xz} \end{bmatrix} \tag{4}$$

Equation (4) defines temperature changes as well as thermal expansion as ΔT and α, respectively. In the case of laminated composites, the elements of the tensor of elasticity are defined as the orthotropic material's lessened elastic constants of the Lth layer, and the next equations express the mentioned relations [84]:

$$\begin{aligned}
C_{11} &= Q_{11}\cos^4\bar{\theta} + 2(Q_{12} + 2Q_{44})\sin^2\bar{\theta}\cos^2\bar{\theta} \\
&\quad + Q_{22}\sin^4\bar{\theta} \\
C_{12} &= (Q_{11} + Q_{22} - 4Q_{44})\sin^2\bar{\theta}\cos^2\bar{\theta} \\
&\quad + Q_{12}(\sin^4\bar{\theta} + \cos^4\bar{\theta}) \\
C_{22} &= Q_{11}\sin^4\bar{\theta} + 2(Q_{12} + 2Q_{44})\sin^2\bar{\theta}\cos^2\bar{\theta} \\
&\quad + Q_{22}\cos^4\bar{\theta} \\
C_{44} &= Q_{44}\cos^4\bar{\theta} + Q_{55}\sin^4\bar{\theta} \\
C_{55} &= Q_{55}\cos^4\bar{\theta} + Q_{66}\sin^4\bar{\theta} \\
C_{66} &= (Q_{11} + Q_{22} - 2Q_{12})\sin^2\bar{\theta}\cos^2\bar{\theta} \\
&\quad + Q_{66}(\cos^2\bar{\theta} - \sin^2\bar{\theta})^2
\end{aligned} \tag{5}$$

The aforementioned equations express the relation between stress and strain components for the Lth orthotropic lamina referred to the lamina's principal material axes x, θ, and z. In Eq (5), Q_{ij} components are expressed by the following equations:

$$\begin{aligned}
&Q_{11} = \frac{E_1}{1-\nu_{12}\nu_{21}}, \quad Q_{12} = \frac{\nu_{12}E_2}{1-\nu_{12}\nu_{21}}, \quad Q_{22} = \frac{E_2}{1-\nu_{12}\nu_{21}} \\
&Q_{66} = G_{12}, \quad Q_{44} = G_{23}, \quad Q_{55} = G_{13}
\end{aligned} \tag{6}$$

2.2 Displacement field

FSDT enables us to define the displacement field of a laminated nanoshell in the following equations [16, 47, 50, 53, 85–91]:

$$\begin{aligned}
U(x,\theta,z,t) &= u(x,\theta,z) + z\psi_x(x,\theta,t) \\
V(x,\theta,z,t) &= v(x,\theta,z) + z\psi_\theta(x,\theta,t) \\
W(x,\theta,z,t) &= w(x,\theta,t)
\end{aligned} \tag{7}$$

Also, $u(x,\theta,t)$, $v(x,\theta,t)$ and $w(x,\theta,t)$, respectively, demonstrate the displacements of the neutral surface in x and θ axes. $\psi_x(x,\theta,t)$ and $\psi_\theta(x,\theta,t)$ illustrate the cross section rotations around θ and x directions. By inserting Eq (7) into Eq (3), the strain tensor's components can be obtained by the following equations:

$$\begin{aligned}
&\varepsilon_{xx} = \frac{\partial u}{\partial x} + z\frac{\partial\psi_x}{\partial x}, \ \varepsilon_{\theta\theta} = \frac{1}{R}\frac{\partial v}{\partial\theta} + \frac{z}{R}\frac{\partial\psi_\theta}{\partial\theta} + \frac{w}{R} \\
&\varepsilon_{xz} = \frac{1}{2}\left(\psi_x + \frac{\partial w}{\partial x}\right), \ \varepsilon_{\theta z} = \frac{1}{2}\left(\psi_\theta + \frac{1}{R}\frac{\partial w}{\partial\theta} - \frac{v}{R}\right) \\
&\varepsilon_{x\theta} = \frac{1}{2}\left(\frac{1}{R}\frac{\partial u}{\partial\theta} + \frac{\partial v}{\partial x}\right) + \frac{z}{2}\left(\frac{1}{R}\frac{\partial\psi_x}{\partial\theta} + \frac{\partial\psi_\theta}{\partial x}\right)
\end{aligned} \tag{8}$$

2.3 Governing equations and boundary conditions

The motion equations along with the possible BCs related to the mentioned structure would be extracted applying energy methods (Hamilton principle) based on FSDT and the NSG model by the following equation:

$$\int_{t_1}^{t_2} (\delta K - \delta \Pi_s + \delta W)\,\mathrm{d}t = 0 \tag{9}$$

where K illustrates the kinetic energy, Π_s defines strain energy and the work done by forces imposed can be shown as Π_w. For a usual nanoshell exposed to high level of temperature situation, it is suggested that the temperature distributes through its thickness.

Based on NSG model, Eq (10) defines the strain energy [83]:

$$\delta K = \int_Z \iint_A \rho \left\{ \begin{array}{l} \left(\frac{\partial u}{\partial t} + z\frac{\partial \psi_x}{\partial t}\right)\left(\frac{\partial}{\partial t}\delta u + z\frac{\partial}{\partial t}\delta\psi_x\right) \\ +\left(\frac{\partial v}{\partial t} + z\frac{\partial \psi_\theta}{\partial t}\right)\left(\frac{\partial}{\partial t}\delta v + z\frac{\partial}{\partial t}\delta\psi_\theta\right) \\ +\left(\frac{\partial w}{\partial t}\right)\frac{\partial}{\partial t}\delta w \end{array} \right\} \mathrm{d}V \tag{10}$$

And also, the strain energy can be defined as the following equation due to the NSG model [83]:

$$\Pi_s = \frac{1}{2}\iiint_V \left(\sigma_{ij}\varepsilon_{ij} + \sigma_{ij}^{(1)}\nabla\varepsilon_{ij}\right)\mathrm{dV}$$
$$\Rightarrow \delta\Pi_s = \iiint_S t_{ij}\delta\varepsilon_{ij}\mathrm{dV} + \iint_A \sigma_{ij}^{(1)}\delta\varepsilon_{ij}\Big|_0^L \mathrm{d}S \tag{11}$$

For a typical isotropic cylindrical shell which is in the high-temperature environment, it is assumed that the temperature can be distributed across its thickness. Hence, the work done depended on the temperature change can be obtained as:

$$\delta W = \iint_A \left[\left(N_2^T\right)\left(\frac{\delta w_0}{\partial x}\right)\frac{\partial w_0}{\partial x} + \left(N_1^T\right)\left(\frac{\delta v_0}{\partial x}\right)\frac{\partial v_0}{\partial x}\right] R\,\mathrm{d}x\,\mathrm{d}\theta \tag{12}$$

where N_1^T and N_2^T are the thermal resultants which can be obtained as follows:

$$N_1^T = \int_{-h_c/2}^{h_c/2} (\bar{Q}_{11} + \bar{Q}_{12})\,\alpha(T - T_0)\mathrm{d}z_c,$$
$$N_2^T = \int_{-h_c/2}^{h_c/2} (\bar{Q}_{21} + \bar{Q}_{22})\,\alpha(T - T_0)\mathrm{d}z_c. \tag{13}$$

It is assumed that the temperature varies linearly along the thickness from T_m at the outer surface to T_c at the inner surface. Governing motion equations for a nanoshell due to the FSDT as well as NSG model are presented inserting Eqs. (10), (12), and (13) into Eq (9) and integrating as follows:

$$\begin{aligned}
\delta u:\ & A_{11}\left(\frac{\partial^2 u}{\partial x^2} + l^2\frac{\partial^4 u}{\partial x^4} - \frac{l^2}{R^2}\frac{\partial^4 u}{\partial x^2\partial\theta^2}\right) + B_{11}\left(\frac{\partial^2\psi_x}{\partial x^2} + l^2\frac{\partial^4\psi_x}{\partial x^4} - \frac{l^2}{R^2}\frac{\partial^4\psi_x}{\partial x^2\partial\theta^2}\right) + B_{12}\frac{1}{R}\frac{\partial^2\psi_\theta}{\partial x\partial\theta} \\
& A_{12}\left(\frac{1}{R}\frac{\partial^2 v}{\partial x\partial\theta} + \frac{1}{R}\frac{\partial w}{\partial x} - \frac{l^2}{R^2}\frac{\partial^4 v}{\partial x^3\partial\theta} - \frac{l^2}{R^2}\frac{\partial^3 w}{\partial x^3} - \frac{l^2}{R^3}\frac{\partial^4 v}{\partial x\partial\theta^3} - \frac{l^2}{R^3}\frac{\partial^3 w}{\partial x\partial\theta^2}\right) - N_h\left(\frac{1}{R}\frac{\partial^2 v}{\partial x\partial\theta} - \frac{1}{R^2}\frac{\partial^2 u}{\partial\theta^2}\right) \\
& + \frac{A_{66}}{R}\left(\frac{1}{R}\frac{\partial^2 u}{\partial\theta^2} + \frac{\partial^2 v}{\partial x\partial\theta} - \frac{l^2}{R}\frac{\partial^4 u}{\partial x^2\partial\theta^2} - l^2\frac{\partial^4 v}{\partial x^3\partial\theta} - \frac{l^2}{R^3}\frac{\partial^4 u}{\partial\theta^4} - \frac{l^2}{R^2}\frac{\partial^4 v}{\partial x\partial\theta^3}\right) + B_{12}\left(-\frac{l^2}{R}\frac{\partial^4\psi_\theta}{\partial x^3\partial\theta} - \frac{l^2}{R^3}\frac{\partial^4\psi_\theta}{\partial x\partial\theta^3}\right) \\
& + \frac{B_{66}}{R}\left(\frac{1}{R}\frac{\partial^2\psi_x}{\partial\theta^2} + \frac{\partial^2\psi_\theta}{\partial x\partial\theta} - \frac{l^2}{R}\frac{\partial^4\psi_x}{\partial x^2\partial\theta^2} - l^2\frac{\partial^4\psi_\theta}{\partial x^3\partial\theta} - \frac{l^2}{R^3}\frac{\partial^4\psi_x}{\partial\theta^4} - \frac{l^2}{R^2}\frac{\partial^4\psi_\theta}{\partial x\partial\theta^3}\right) = (1-\mu^2\nabla^2)\left(I_0\frac{\partial^2 u}{\partial t^2} + I_1\frac{\partial^2\psi_x}{\partial t^2}\right)
\end{aligned} \tag{14}$$

$$\begin{aligned}
\delta v:\ & \frac{A_{12}}{R}\left(\frac{\partial^2 u}{\partial x\partial\theta} + l^2\frac{\partial^4 u}{\partial x^3\partial\theta} - \frac{l^2}{R^2}\frac{\partial^4 u}{\partial x\partial\theta^3}\right) + \frac{B_{12}}{R}\left(\frac{\partial^2\psi_x}{\partial x\partial\theta} + l^2\frac{\partial^4\psi_x}{\partial x^3\partial\theta} - \frac{l^2}{R^2}\frac{\partial^4\psi_x}{\partial x\partial\theta^3}\right) - (1-\nabla^2 l^2)N_1^T\frac{\partial^2 v}{\partial x^2} \\
& \frac{A_{22}}{R}\left(\frac{1}{R}\frac{\partial^2 v}{\partial\theta^2} + \frac{1}{R}\frac{\partial w}{\partial\theta} - \frac{l^2}{R^2}\frac{\partial^4 v}{\partial x^2\partial\theta^2} - \frac{l^2}{R^2}\frac{\partial^3 w}{\partial x^2\partial\theta} - \frac{l^2}{R^3}\frac{\partial^4 v}{\partial\theta^4} - \frac{l^2}{R^3}\frac{\partial^3 w}{\partial\theta^3}\right) - A_{66}\frac{l^2}{R^2}\frac{\partial^4 v}{\partial x^2\partial\theta^2} \\
& + \frac{B_{22}}{R}\left(\frac{1}{R}\frac{\partial^2\psi_\theta}{\partial\theta^2} + \frac{l^2}{R}\frac{\partial^4\psi_\theta}{\partial x^2\partial\theta^2} - \frac{l^2}{R^3}\frac{\partial^4\psi_\theta}{\partial\theta^4}\right) + A_{66}\left(\frac{1}{R}\frac{\partial^2 u}{\partial x\partial\theta} + \frac{\partial^2 v}{\partial x^2} - \frac{l^2}{R}\frac{\partial^4 u}{\partial x^3\partial\theta} - l^2\frac{\partial^4 v}{\partial x^4} - \frac{l^2}{R^3}\frac{\partial^4 u}{\partial x\partial\theta^3}\right) \\
& + B_{66}\left(\frac{1}{R}\frac{\partial^2\psi_x}{\partial x\partial\theta} + \frac{\partial^2\psi_\theta}{\partial x^2} - \frac{l^2}{R}\frac{\partial^4\psi_x}{\partial x^3\partial\theta} - l^2\frac{\partial^4\psi_\theta}{\partial x^4} - \frac{l^2}{R^3}\frac{\partial^4\psi_x}{\partial x\partial\theta^3} - \frac{l^2}{R^2}\frac{\partial^4\psi_\theta}{\partial x^2\partial\theta^2}\right) \\
& + \frac{K_s A_{44}}{R}\left(\psi_\theta + \frac{1}{R}\frac{\partial w}{\partial\theta} - \frac{v}{R} - l^2\frac{\partial^2\psi_\theta}{\partial x^2} - \frac{l^2}{R^2}\frac{\partial^3 w}{\partial x^2\partial\theta} + \frac{l^2}{R^2}\frac{\partial^2 v}{\partial x^2} - \frac{l^2}{R^2}\frac{\partial^2\psi_\theta}{\partial\theta^2} - \frac{l^2}{R^3}\frac{\partial^3 w}{\partial\theta^3} + \frac{l^2}{R^3}\frac{\partial^2 v}{\partial\theta^2}\right) \\
& = \left(1-\mu^2\nabla^2\right)\left(I_0\left[\frac{\partial^2 v}{\partial t^2}\right] + I_1\left[\frac{\partial^2\psi_\theta}{\partial t^2}\right]\right)
\end{aligned} \tag{15}$$

$$\begin{aligned}
\delta w:\ &\frac{A_{12}}{R}\left(\frac{\partial u}{\partial x}+l^2\frac{\partial^3 u}{\partial x^3}+\frac{l^2}{R^2}\frac{\partial^3 u}{\partial x\partial\theta^2}\right)+\frac{B_{12}}{R}\left(\frac{\partial\psi_x}{\partial x}+l^2\frac{\partial^3\psi_x}{\partial x^3}+\frac{l^2}{R^2}\frac{\partial^3\psi_x}{\partial x\partial\theta^2}\right)\\
&-(1-\nabla^2 l^2)N_2^T\frac{\partial^2 w}{\partial x^2}\frac{A_{22}}{R}\left(-\frac{1}{R}\frac{\partial v}{\partial\theta}-\frac{w}{R}+\frac{l^2}{R^2}\frac{\partial^3 v}{\partial x^2\partial\theta}+\frac{l^2}{R^2}\frac{\partial^2 w}{\partial x^2}+\frac{l^2}{R^3}\frac{\partial^3 v}{\partial\theta^3}+\frac{l^2}{R^3}\frac{\partial^2 w}{\partial\theta^2}\right)\\
&+\frac{B_{22}}{R}\left(-\frac{1}{R}\frac{\partial\psi_\theta}{\partial\theta}+\frac{l^2}{R^2}\frac{\partial^3\psi_\theta}{\partial x^2\partial\theta}+\frac{l^2}{R^3}\frac{\partial^3\psi_\theta}{\partial\theta^3}\right)\\
&+K_sA_{55}\left(\frac{\partial\psi_x}{\partial x}-\frac{\partial^2 w}{\partial x^2}-l^2\frac{\partial^3\psi_x}{\partial x^3}-l^2\frac{\partial^4 w}{\partial x^4}-\frac{l^2}{R^2}\frac{\partial^3\psi_x}{\partial x\partial\theta^2}-\frac{l^2}{R^2}\frac{\partial^4 w}{\partial x^2\partial\theta^2}\right)\\
&+\frac{K_sA_{44}}{R}\left(\frac{\partial\psi_\theta}{\partial\theta}-\frac{1}{R}\frac{\partial^2 w}{\partial\theta^2}-\frac{1}{R}\frac{\partial v}{\partial\theta}-l^2\frac{\partial^3\psi_\theta}{\partial x^2\partial\theta}-\frac{l^2}{R}\frac{\partial^4 w}{\partial x^2\partial\theta^2}+\frac{l^2}{R}\frac{\partial^3 v}{\partial x^2\partial\theta}-\frac{l^2}{R^2}\frac{\partial^3\psi_\theta}{\partial\theta^3}-\frac{l^2}{R^3}\frac{\partial^4 w}{\partial\theta^4}+\frac{l^2}{R^3}\frac{\partial^3 v}{\partial\theta^3}\right)\\
&=\left(1-\mu^2\nabla^2\right)\left(I_0\left(\frac{\partial^2 w}{\partial t^2}\right)\right)
\end{aligned}\tag{16}$$

$$\begin{aligned}
\delta\psi_x:\ &B_{11}\left(\frac{\partial^2 u}{\partial x^2}-l^2\frac{\partial^4 u}{\partial x^4}-\frac{l^2}{R^2}\frac{\partial^4 u}{\partial x^2\partial\theta^2}\right)+D_{11}\left(\frac{\partial^2\psi_x}{\partial x^2}-l^2\frac{\partial^4\psi_x}{\partial x^4}-\frac{l^2}{R^2}\frac{\partial^4\psi_x}{\partial x^2\partial\theta^2}\right)\\
&+B_{12}\left(\frac{1}{R}\frac{\partial^2 v}{\partial x\partial\theta}+\frac{1}{R}\frac{\partial w}{\partial x}-\frac{l^2}{R^2}\frac{\partial^4 v}{\partial x^3\partial\theta}-\frac{l^2}{R^2}\frac{\partial^3 w}{\partial x^3}-\frac{l^2}{R^3}\frac{\partial^4 v}{\partial x\partial\theta^3}-\frac{l^2}{R^3}\frac{\partial^3 w}{\partial x\partial\theta^2}\right)+D_{12}\left(-\frac{l^2}{R^3}\frac{\partial^4 u}{\partial\theta^4}-\frac{l^2}{R^2}\frac{\partial^4 v}{\partial x\partial\theta^3}\right)\\
&+D_{12}\left(\frac{1}{R}\frac{\partial^2\psi_\theta}{\partial x\partial\theta}+\frac{l^2}{R^2}\frac{\partial^4\psi_\theta}{\partial x^3\partial\theta}-\frac{l^2}{R^3}\frac{\partial^4\psi_\theta}{\partial x\partial\theta^3}\right)+\frac{B_{66}}{R}\left(\frac{1}{R}\frac{\partial^2 u}{\partial\theta^2}+\frac{\partial^2 v}{\partial x\partial\theta}-\frac{l^2}{R}\frac{\partial^4 u}{\partial x^2\partial\theta^2}-l^2\frac{\partial^4 v}{\partial x^3\partial\theta}\right)\\
&+\frac{D_{66}}{R}\left(\frac{1}{R}\frac{\partial^2\psi_x}{\partial\theta^2}+\frac{\partial^2\psi_\theta}{\partial x\partial\theta}-\frac{l^2}{R}\frac{\partial^4\psi_x}{\partial x^2\partial\theta^2}-l^2\frac{\partial^4\psi_\theta}{\partial x^3\partial\theta}-\frac{l^2}{R^3}\frac{\partial^4\psi_x}{\partial\theta^4}-\frac{l^2}{R^2}\frac{\partial^4\psi_\theta}{\partial x\partial\theta^3}\right)\\
&-K_sA_{55}\left(\psi_x+\frac{\partial w}{\partial x}-l^2\frac{\partial^2\psi_x}{\partial x^2}-l^2\frac{\partial^3 w}{\partial x^3}-\frac{l^2}{R^2}\frac{\partial^2\psi_x}{\partial\theta^2}-\frac{l^2}{R^2}\frac{\partial^3 w}{\partial x\partial\theta^2}\right)=(1-\mu^2\nabla^2)\left(I_1\frac{\partial^2 u}{\partial t^2}+I_2\frac{\partial^2\psi_x}{\partial t^2}\right)
\end{aligned}\tag{17}$$

$$\begin{aligned}
\delta\psi_\theta:\ &\frac{B_{12}}{R}\left(\frac{\partial^2 u}{\partial x\partial\theta}-l^2\frac{\partial^4 u}{\partial x^3\partial\theta}-\frac{l^2}{R^2}\frac{\partial^4 u}{\partial x\partial\theta^3}\right)+\frac{D_{12}}{R}\left(\frac{\partial^2\psi_x}{\partial x\partial\theta}-l^2\frac{\partial^4\psi_x}{\partial x^3\partial\theta}-\frac{l^2}{R^2}\frac{\partial^4\psi_x}{\partial x\partial\theta^3}\right)\\
&+\frac{B_{22}}{R}\left(\frac{1}{R}\frac{\partial^2 v}{\partial\theta^2}-\frac{1}{R}\frac{\partial w}{\partial\theta}-\frac{l^2}{R^2}\frac{\partial^4 v}{\partial x^2\partial\theta^2}-\frac{l^2}{R^2}\frac{\partial^3 w}{\partial x^2\partial\theta}-\frac{l^2}{R^3}\frac{\partial^4 v}{\partial\theta^4}-\frac{l^2}{R^3}\frac{\partial^3 w}{\partial\theta^3}\right)+\frac{D_{22}}{R}\left(\frac{1}{R}\frac{\partial^2\psi_\theta}{\partial\theta^2}-\frac{l^2}{R}\frac{\partial^4\psi_\theta}{\partial x^2\partial\theta^2}\right)\\
&+B_{66}\left(\frac{1}{R}\frac{\partial^2 u}{\partial x\partial\theta}-\frac{\partial^2 v}{\partial x^2}-\frac{l^2}{R}\frac{\partial^4 u}{\partial x^3\partial\theta}-l^2\frac{\partial^4 v}{\partial x^4}-\frac{l^2}{R^3}\frac{\partial^4 u}{\partial x\partial\theta^3}-\frac{l^2}{R^2}\frac{\partial^4 v}{\partial x^2\partial\theta^2}\right)-\frac{D_{22}}{R}\frac{l^2}{R^3}\frac{\partial^4\psi_\theta}{\partial\theta^4}\\
&+D_{66}\left(\frac{1}{R}\frac{\partial^2\psi_x}{\partial x\partial\theta}-\frac{\partial^2\psi_\theta}{\partial x^2}-\frac{l^2}{R}\frac{\partial^4\psi_x}{\partial x^3\partial\theta}-l^2\frac{\partial^4\psi_\theta}{\partial x^4}-\frac{l^2}{R^3}\frac{\partial^4\psi_x}{\partial x\partial\theta^3}-\frac{l^2}{R^2}\frac{\partial^4\psi_\theta}{\partial x^2\partial\theta^2}\right)\\
&-k_sA_{44}\left(\psi_\theta+\frac{1}{R}\frac{\partial w}{\partial\theta}-\frac{v}{R}-l^2\frac{\partial^2\psi_\theta}{\partial x^2}-\frac{l^2}{R}\frac{\partial^3 w}{\partial x^2\partial\theta}+\frac{l^2}{R}\frac{\partial^2 v}{\partial x^2}-\frac{l^2}{R^2}\frac{\partial^2\psi_\theta}{\partial\theta^2}-\frac{l^2}{R^3}\frac{\partial^3 w}{\partial\theta^3}+\frac{l^2}{R^3}\frac{\partial^2 v}{\partial\theta^2}\right)\\
&=\left(1-\mu^2\nabla^2\right)\left[I_1\left(\frac{\partial^2 v}{\partial t^2}\right)+I_2\left(\frac{\partial^2\psi_\theta}{\partial t^2}\right)\right]
\end{aligned}\tag{18}$$

where the defined elements in Eqs. (14) - (18) are explained as:

$$\begin{aligned}
\{A_{11}\ A_{12}\ A_{22}\ A_{66}\ A_{44}\ A_{55}\} &= \int_{-h/2}^{h/2} \{C_{11}\ C_{12}\ C_{22}\ C_{66}\ C_{44}\ C_{55}\}\,\mathrm{d}z \\
\{B_{11}\ B_{12}\ B_{22}\ B_{66}\} &= \int_{-h/2}^{h/2} \{C_{11}\ C_{12}\ C_{22}\ C_{66}\}\,z\mathrm{d}z \\
\{D_{11}\ D_{12}\ D_{22}\ D_{66}\} &= \int_{-h/2}^{h/2} \{C_{11}\ C_{12}\ C_{22}\ C_{66}\}\,z^2\mathrm{d}z \\
\{I_0\ I_1\ I_2\} &= \int_{-h/2}^{h/2} \rho(z,T)\{1\ z\ z^2\}\,z\mathrm{d}z
\end{aligned} \tag{19}$$

3 Solution procedure

One of the best numerical methods which is well known for its accuracy and convergence is differential quadrature method (DQM) [92–94]. In this method, it is really important that the numbers of seed should be optimal; it means that due to an increase in the computational charge, too many seeds or elements are not applicable; and employing the few seeds, however, would lead to a negative impact on accuracy of the results [95–105]. At first, this method encounters its users with a limitation which they could not use too many seed owning to the weighting function was algebraic. GDQEM is employed with the aim of finding the solutions of governing equations beneath various boundary conditions (Fig. 2). The flowchart of the aforementioned solution method is as below:

With a view of this method, the estimated rth is defined by $f(x)$ as follows:

$$\left.\frac{\partial^r f(x)}{\partial x^r}\right|_{x=x_p} = \sum_{j=1}^{n} C_{ij}^{(r)} f(x_i) \tag{20}$$

n and Cij are the number of seeds and weighting coefficients in order that the second one is computed as below:

$$\begin{aligned}
&C_{ij}^{(1)} = \frac{M(x_i)}{(x_i - x_j)M(x_j)}, \\
&i,j = 1,2,\ldots,n \text{ and } i \neq j \\
&C_{ij}^{(1)} = -\sum_{j=1, i\neq j}^{n} C_{ij}^{(1)},\ i = j
\end{aligned} \tag{21}$$

where

$$M(x_i) = \prod_{j=1, j\neq i}^{n} (x_i - x_j) \tag{22}$$

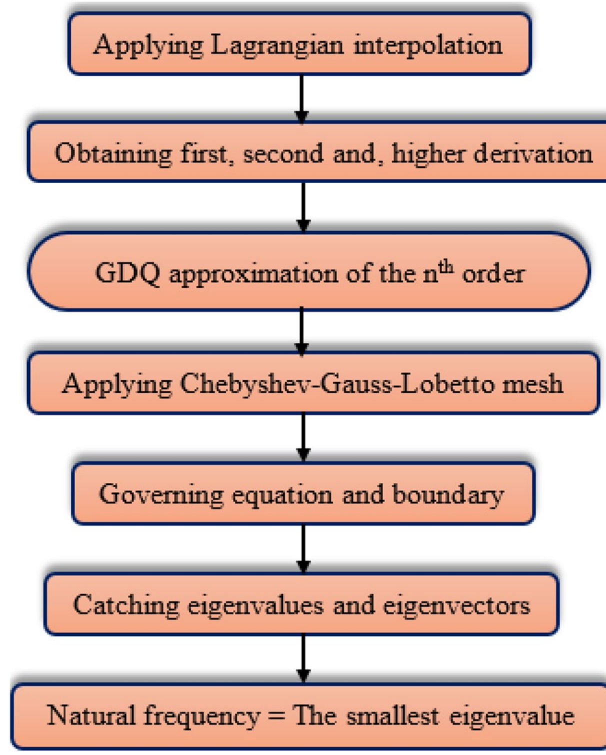

Fig. 2 The flowchart of GDQEM

Also, these higher-order weight coefficients are as follows:

$$\begin{aligned}
&C_{ij}^{(r)} = r\left[C_{ij}^{(r-1)} C_{ij}^{(1)} - \frac{C_{ij}^{(r-1)}}{(x_i - x_j)}\right] \\
&i,j = 1,2,\ldots,n, i \neq j \text{ and } 2 \le r \le n-1 \\
&C_{ii}^{(r)} = -\sum_{j=1, i\neq j}^{n} C_{ij}^{(r)} \\
&i,j = 1,2,\ldots,n \text{ and } 1 \le r \le n-1
\end{aligned} \tag{23}$$

In the present research investigation, a seeds' nonuniform set is chosen along x and θ excess:

$$x_i = \frac{L}{2}\left(1 - \cos\left(\frac{(i-1)}{(N_i - 1)}\pi\right)\right), \quad i = 1,2,3,\ldots,N_i \tag{24}$$

The freedom degrees can be taken into consideration as follows:

$$\begin{aligned}
u(x,\theta,t) &= U(x)\cos(n\theta)e^{i\omega t}, \\
v(x,\theta,t) &= V(x)\sin(n\theta)e^{i\omega t}, \\
w(x,\theta,t) &= W(x)\cos(n\theta)e^{i\omega t}, \\
\psi_x(x,\theta,t) &= \Psi_x(x)\cos(n\theta)e^{i\omega t}, \\
\psi_\theta(x,\theta,t) &= \Psi_\theta(x)\sin(n\theta)e^{i\omega t}.
\end{aligned}$$

Reorganizing the quadrature analogs of boundary conditions along with field equations into the generalized eigenvalue problem's fabric, we obtain:

$$\left\{\left[\begin{bmatrix}M_{dd}\\M_{bd}\end{bmatrix}\begin{bmatrix}M_{db}\\M_{bb}\end{bmatrix}\right]\omega^2+\left[\begin{bmatrix}K_{dd}\\K_{bd}\end{bmatrix}\begin{bmatrix}K_{db}\\K_{bb}\end{bmatrix}\right]\right\}\left\{\begin{matrix}\delta_d\\\delta_b\end{matrix}\right\}=0 \quad (25)$$

where the subscripts d and b are pertained to the grid points' domain and boundary, respectively. Also, displacement vector is shown by δ. Equation (25), however, may be changed to a basic problem of eigenvalue:

$$\begin{aligned}[K^*]\{\delta_i\} &= (\omega^2)[M^*]\{\delta_i\}\\ [K^*] &= [K_{dd}-K_{db}K_{bb}^{-1}K_{bd}]\\ [M^*] &= [M_{dd}-M_{db}K_{bb}^{-1}K_{bd}]\end{aligned} \quad (26)$$

Also, dimensionless natural frequency and dimensionless temperature difference are defined as follows:

$$\Omega = 10\times\omega L(\sqrt{\frac{\rho}{E}}) \quad (27)$$

4 Results section

In this paper, the laminated composite nanoshell's material properties are given in Table 1. The most prominent superiority of AS/3501 composite compared with conventional composites is their higher stiffness and strength as well as less density [106].

4.1 Convergence

A sufficient number of grid points are necessary to achieve accurate results in GDQM [20, 44, 107–127]. The convergence studies are conducted for different boundary conditions as well as different materials. Moreover, it can be seen that the structure with (C–C) boundary conditions is stiffer than the structure with C–F boundary conditions which will lead to a smaller natural frequency. Also, GPLRC cylindrical nanoshell, due to the addition of GPL reinforcing nanofillers, has a higher natural frequency in comparison with pure epoxy. According to Table 2, for results convergence, thirteen grid points are suitable.

4.2 Validation

For results verification of this work with other articles, Table 3 gives a comparison of results for dimensionless natural frequency of the nanostructure with the results of Ref [128], for different geometrical parameters. Moreover, the results reveal that the decrease in dimensionless length scale parameter (*h/l*) would lead to the reduction of the dimensionless natural frequency. In order to validate the proposed formulation, some comparative studies are conducted between the obtained results in this study and those available in the literature. Table 3 shows that there is a very good agreement between the results.

5 The effects of length scale parameter and temperature on the frequency for different boundary conditions

Figures 3, 4 and 5 present the effect of length scale parameter (l) on the dimensionless frequency with different boundary conditions. In this study, for reliability of result four quantities are considered for l ($l=0.1$, 0.15, 0.2 and 0.25 nm). It is observed that for $l=0.25$ nm dimensionless frequency was higher in all the boundary conditions that evaluated; also, for this among of l critical temperature was more, compare other one. It can be seen from figures that an increase in the l causes an increase in the critical temperature and increases the stability of the nanostructure. Also, it can be observed that by increasing temperature, frequency has been decreased. This is because increasing the temperature is eventuated to decrease the stiffness and frequency of the nanostructure. When one draws a comparison between

Table 1 The effect of the number of grid points on the results convergence for the dimensionless frequency of the GNPRC micropanel with respect to different patterns and boundary conditions (B.Cs) when a/b = 6.5, h = a/9, R1 = R2 = 10a, Δ T = 10 (K), $g_{GPL}=0.5\%$

		$N=M=7$	$N=M=9$	$N=M=11$	$N=M=13$	$N=M=15$
CFFF	Pure epoxy	0.0152839	0.0171311	0.0122786	**0.0184308**	**0.0185104**
	Pattern 2	0.0320457	0.0333990	0.0379272	**0.0340140**	**0.0340840**
CSFS	Pure epoxy	0.0245107	0.0279184	**0.0205209**	**0.0205209**	0.0205209
	Pattern 2	0.0411726	0.0410866	**0.0407444**	**0.0407444**	0.0407444
SSSS	Pure epoxy	0.0328041	**0.0328039**	**0.0328039**	0.0328039	0.0328039
	Pattern 2	**0.0685672**	**0.06850382**	0.06844328	0.06839187	0.0683808
CSSS	Pure epoxy	0.0551124	0.05553747	0.05366811	**0.05552384**	**0.0555205**
	Pattern 2	0.0971378	0.0989422	0.09917005	**0.09929541**	**0.0992978**
CCCC	Pure epoxy	0.0763170	0.0763555	**0.0763567**	**0.0763567**	0.0763567
	Pattern 2	0.1388539	0.13889832	0.13889978	0.1389035	0.1389035

Table 2 The material properties of AS/3501 graphite–epoxy layers [84]

Material properties	E_1	E_2	G_{12}	G_{13}	G_{23}	α_1	α_2	ν_s
Values	140GPa	10GPa	7 GPa	7 GPa	7 GPa	$-0.3 \times 10^{-6}/K$	$28 \times 10^{-6}/K$	0.078

Table 3 Comparison of dimensionless first three natural frequencies of isotropic homogeneous nanostructure, with different thicknesses

h/R	n	Ref. [128] (l=0)	Present (l=0)	Ref. [128] (l=h)	Present study (l=h)
0.02	1	0.1954	0.19536215	0.1955	0.19543206
	2	0.2532	0.25271274	0.2575	0.25731258
	3	0.2772	0.27580092	0.3067	0.30621690
0.05	1	0.1959	0.19542305	0.1963	0.19585782
	2	0.2623	0.25884786	0.2869	0.28543902
	3	0.3220	0.31407326	0.4586	0.45457555

Figs. 3, 4 and 5, it can be inferred that while a boundary condition changes from clamp to simply, both frequencies and critical temperature decrease. This results in a decrease in the stability of the nanostructure.

6 The effects of nonlocal parameter and temperature on the frequency for different boundary conditions

The dimensionless temperature versus the dimensionless natural frequency for different nonlocal parameters and S–S, C–S and C–C boundary conditions is depicted in Figs. 6, 7 and 8, respectively. It can be observed that by increasing temperature, dynamic stability of the nanostructure has been decreased as long as critical temperature is seen. As a best result for the literature, it is seen that increasing in the dimensionless nonlocal parameter doesn't have any effects on the critical temperature for each boundary condition. The difference between Figs. 6, 7 and 8 is that, for a specific value of dimensionless nonlocal parameter, the critical temperature and dimensionless frequency of C–C boundary conditions are higher than S–S and C–S boundary conditions. It is clear from these figures that nonlocal parameter and temperature have a same or direct effect on the dynamic stability (dimensionless frequency) of the nanostructure but nonlocal parameter doesn't show any effects on the static stability (critical temperature) of the cylindrical nanoshell.

6.1 The effects of different length to radius ratio on the frequency for different boundary conditions and between odd- and even-layered laminates

From Figs. 9, 10 and 11, it can be observed that three-layered [0° 90° 0°] laminated composite has the lowest value of the critical dimensionless temperature. In addition, the highest value of the critical temperature occurs in the six-layered

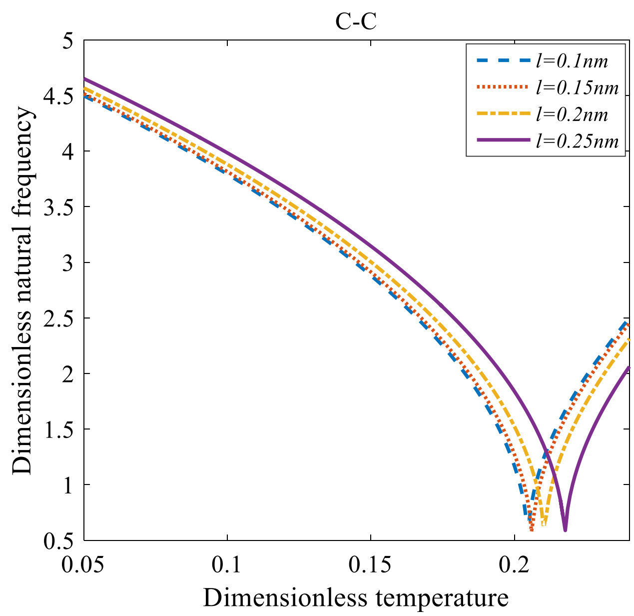

Fig. 3 The effects of l and temperature of environment on the frequency for C–C boundary conditions

[0° 90° 0° 90° 0° 90°] laminated composite. Another significant result is that four-layered [0° 90° 0° 90°] has the higher critical temperature than five-layered [0° 90° 0° 90° 0°] laminated composite nanostructure. It can be seen that increasing the number of layers causes the critical temperature to increase. It can be concluded from the results that the number of layers has a significant effect on the critical temperature of the laminated composite nanostructure.

6.2 Influences of length scale parameter on the frequency of the laminated composite nanostructure

Figures 12, 13, 14, 15, 16, 17, 18 and 19 show the effect of the different symmetric laminate angle, the number of layers

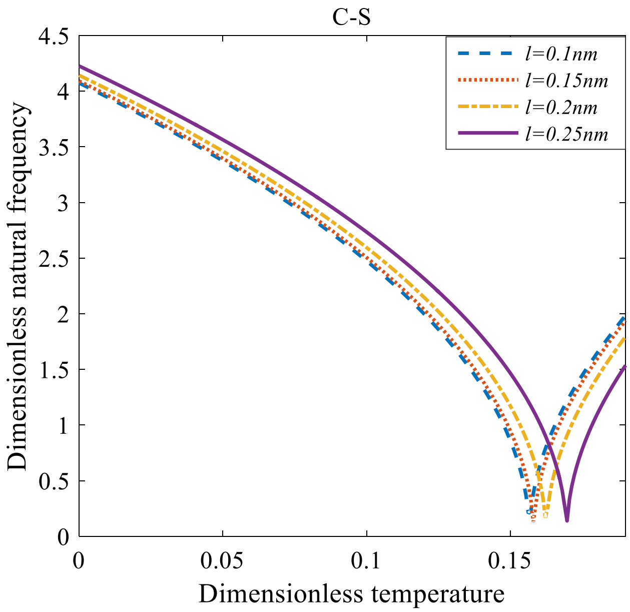

Fig. 4 The effects of l and temperature of environment on the frequency for C–S boundary conditions

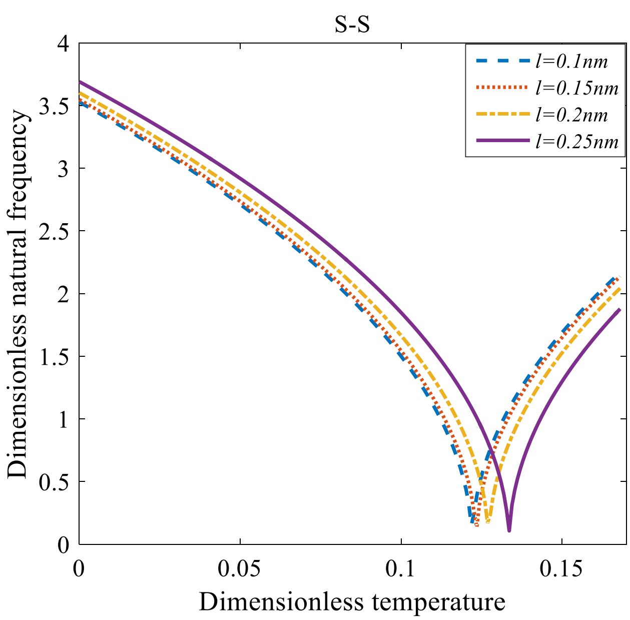

Fig. 5 The effects of l and temperature of environment on the frequency for S–S boundary conditions

and length scale parameter on the frequency for different boundary conditions. The intended model is a laminated composite cylindrical nanoshell in a thermal environment with $\Delta T = 100$, $R = 1$ nm and $h = R/10$. The size-dependent parameters are assumed to be $\mu = 0.55$ nm, $l = 0.35$ nm in the relevant theories [83].

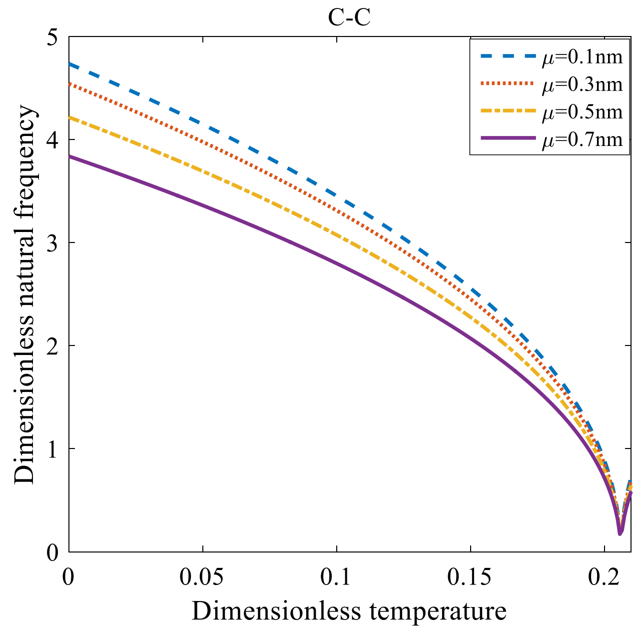

Fig. 6 The effects of μ and temperature of environment on the frequency for C–C boundary conditions

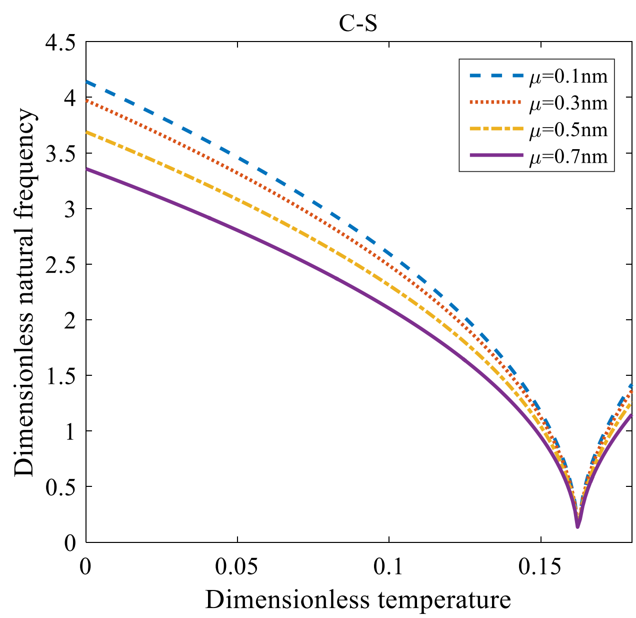

Fig. 7 The effects of μ and temperature of environment on the frequency for C–S boundary conditions

6.3 The comparison between the even-layered laminates

According to Figs. 12, 13, 14 and 15, for C–C, C–S and S–S boundary conditions, increasing the length scale parameter, all the figures demonstrate a similar behavior. By increasing the length scale parameter, the frequency of

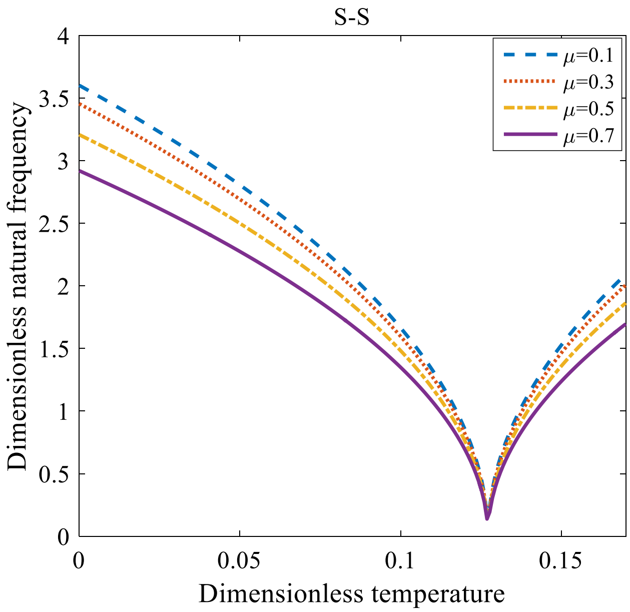

Fig. 8 The effects of μ and temperature of environment on the frequency for S–S boundary conditions

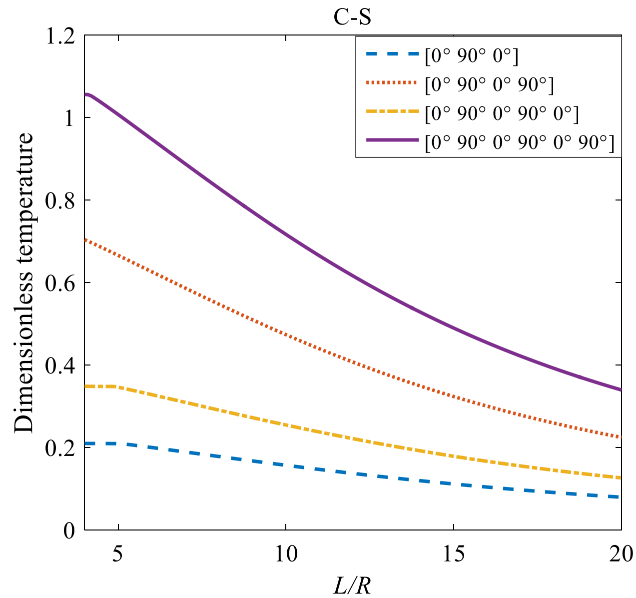

Fig. 10 The effects of L/R and the number of layers on the frequency for C–S boundary conditions

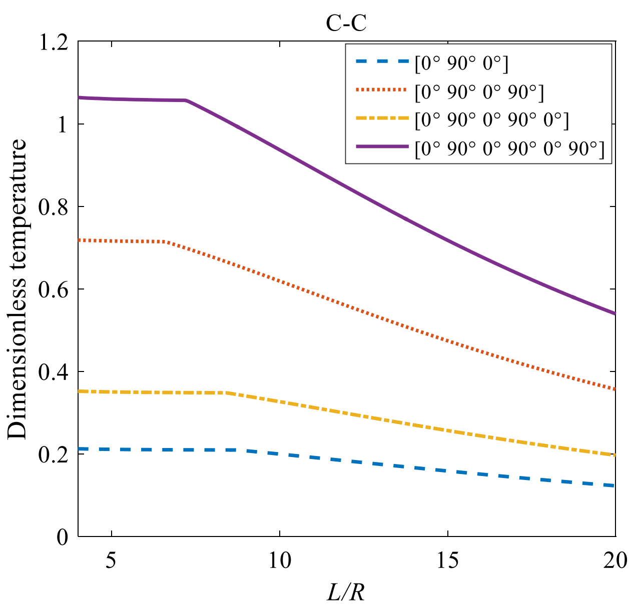

Fig. 9 The effects of L/R and the number of layers on the frequency for C–C boundary conditions

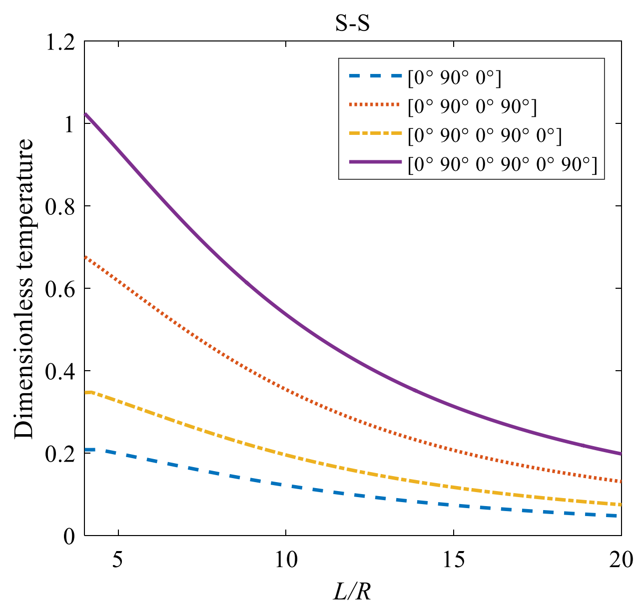

Fig. 11 The effects of L/R and the number of layers on the frequency for S–S boundary conditions

the nanostructure increases. These figures present that by boosting the even layers' number of the laminated composite, the frequency of the structure increases. This increment is remarkable for C–C boundary conditions and improves the structure stability. The difference between Figs. 12, 13 and 14 is that the dimensionless frequency of C–C boundary condition is higher than S–S and C–S boundary conditions. This is because C–C boundary condition improves the nanostructure stability. In addition, for C–F boundary condition, Fig. 15 presents a new result. For this regard, it can be seen that the effect of length scale parameter on the frequency is much more changeable. Moreover, for every even layers' number, in the lower value of length scale parameter, by increasing the length scale parameter, the frequency of

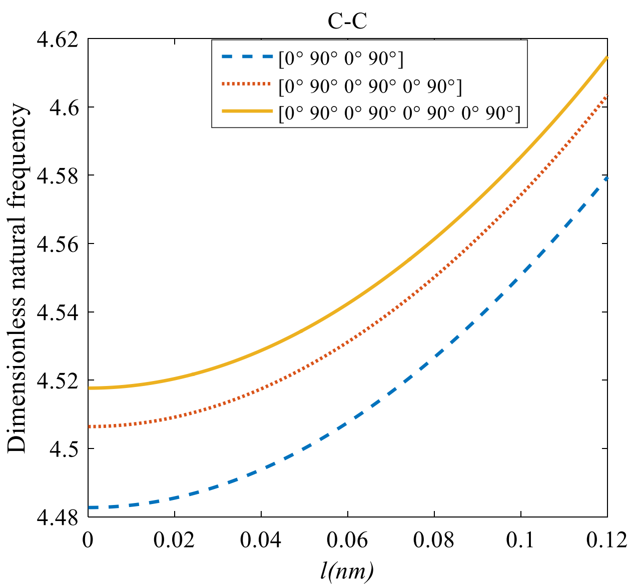

Fig. 12 The effects of l and even layers' number on the frequency for C–C boundary conditions

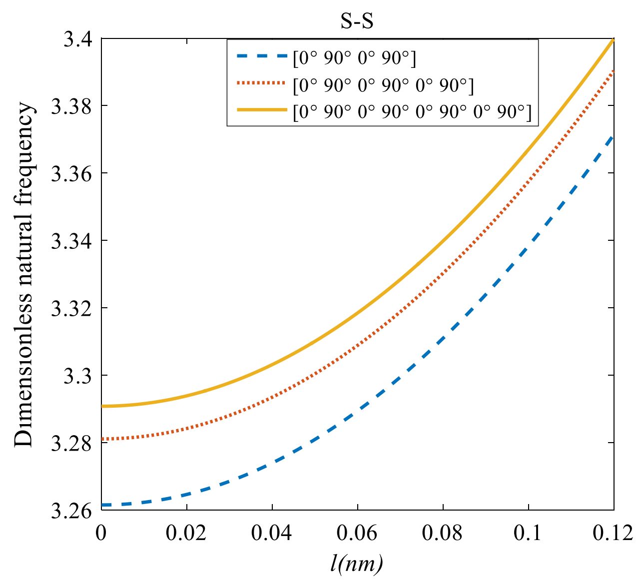

Fig. 14 The effects of l and even layers' number on the frequency for S–S boundary conditions

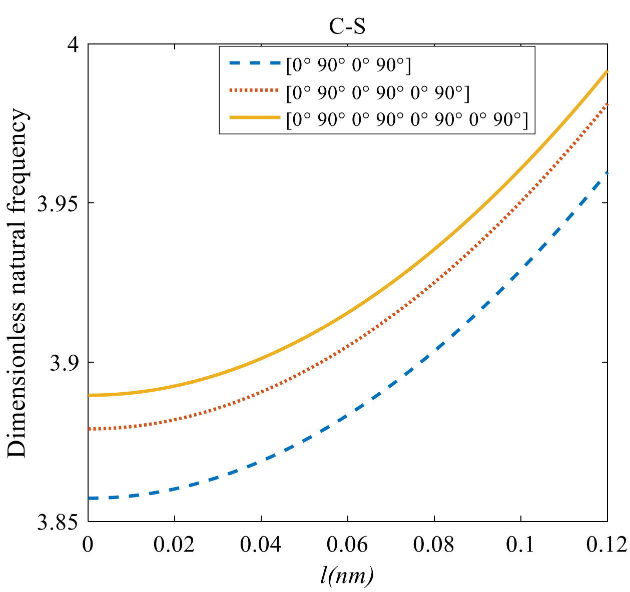

Fig. 13 The effects of l and even layers' number on the frequency for C–S boundary conditions

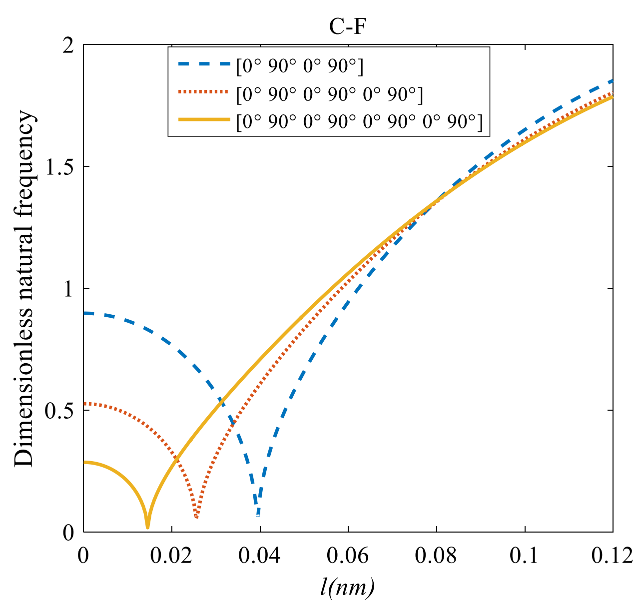

Fig. 15 The effects of l and even layers' number on the frequency for C–F boundary conditions

the structure decreases but in the higher value of length scale parameter this matter is inverse. In addition, this figure shows that even layers' number effect on the frequency, change in $l = 0.872$ nm. So, for length scale parameter less than 0.872 nm, by increasing the number of the composite layers, the frequency increases, while for $l > 0.872$ nm the reverse is true.

6.4 The comparison between the odd-layered laminates

The dimensionless frequency versus the length scale parameter for different odd layers' numbers of the laminated composite and S–S, C–S, C–C and C–F boundary conditions is depicted in Figs. 16, 17, 18 and 19. It is seen that increasing

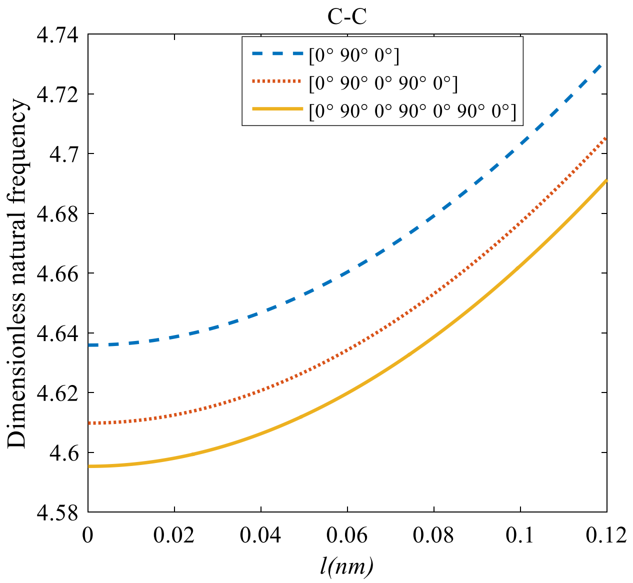

Fig. 16 The effects of l and odd layers' number on the frequency for C–C boundary conditions

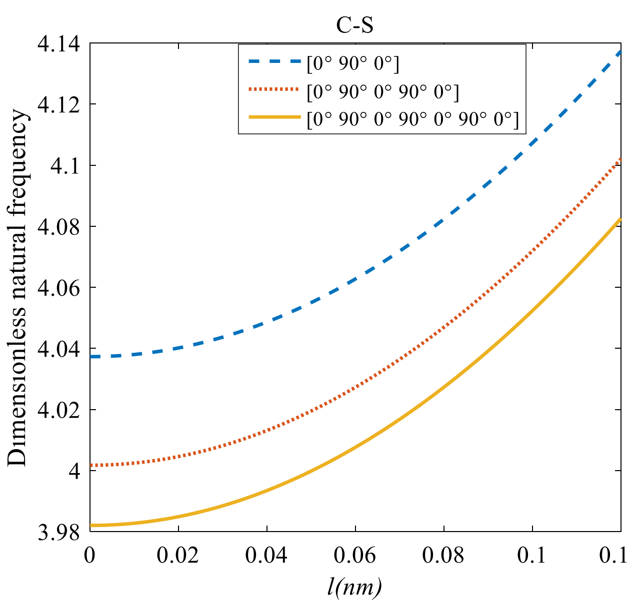

Fig. 17 The effects of l and odd layers' number on the frequency for C–S boundary conditions

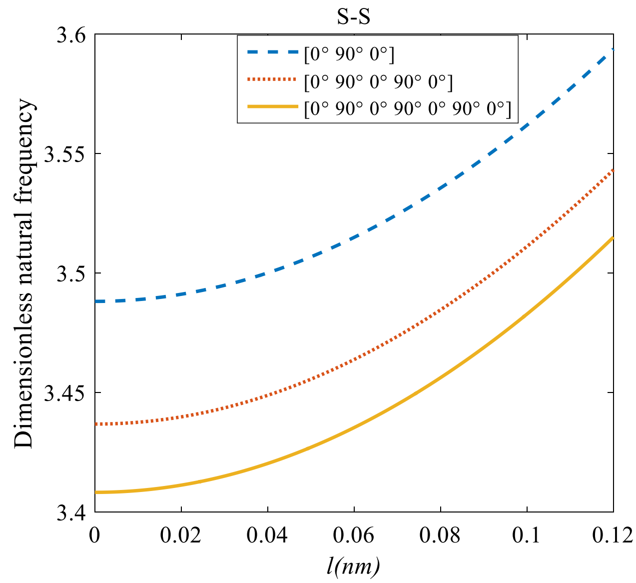

Fig. 18 The effects of l and odd layers' number on the frequency for S–S boundary conditions

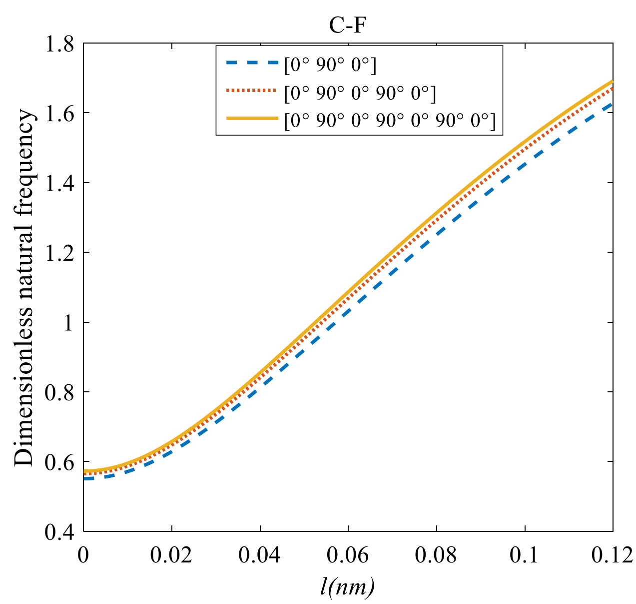

Fig. 19 The effects of l and odd layers' number on the frequency for C–F boundary conditions

length scale parameter causes the frequency of the system to increase. It is clear from Figs. 16, 17, 18 and 19 that because of an increase in stiffness of structure with rising odd layers' number, the variation of frequency with an increase in odd layers' number decreases. As mentioned earlier, by increasing the length scale parameter, the dynamic stability is enhanced. This enhancement is more significant in C–C boundary condition. The difference between these figures is that the effects of odd layers' number on the frequency of the structure with C–F boundary condition are much less than in comparison with others boundary conditions. For more comprehensive, it is true that the odd layers' number has a positive effect on the frequency of the cylindrical nanoshell with C–F boundary condition, but this effect is very little and can be ignored.

7 Conclusion

This article investigated the thermal buckling and stability analysis of a size-dependent laminated composite cylindrical nanoshell in thermal environment using NSGT. The governing equations of the laminated composite cylindrical nanoshell in thermal environment have been derived using Hamilton's principle and solved with the assistance of the GDQEM. In the current study and for the first time, the critical temperature and dynamic stability analysis of a laminated composite cylindrical nanoshell in thermal environment are examined based on an exact continuum theory. Finally, using mentioned continuum mechanics theory, the investigation has been made into the influence of the temperature difference and the different types of the laminated composite on the vibrational characteristics of the nanostructure. In this work, the following main results have been achieved.

1. For C–F boundary conditions and every even layers' number, in the lower value of length scale parameter, by increasing the length scale parameter, the frequency of the structure decreases but in the higher value of length scale parameter this matter is inverse.
2. For C–F boundary conditions and even layers' number, the effects of length scale parameter on the frequency is much more changeable.
3. For C–C, C–S and S–S boundary conditions and every even and odd layers' number, by increasing the length scale parameter and layers' number, the frequency of the structure increases.
4. The results show that the odd layers' number has a positive effect on the frequency of the cylindrical nanoshell with C–F boundary conditions, but this effect is very little and can be ignored.
5. Nonlocal parameter and temperature have a direct effect on the natural frequency of the cylindrical nanoshell, but nonlocal parameter doesn't show any effects on the critical temperature of the cylindrical nanoshell.
6. The number of layers has a positive effect on the critical temperature of the laminated composite cylindrical nanoshell.

Acknowledgments The research described in this paper was financially supported by the Natural Science Foundation.

References

1. Nadri S, Xie L, Jafari M, Alijabbari N, Cyberey ME, Barker NS et al. (2018) A 160 GHz frequency Quadrupler based on heterogeneous integration of GaAs Schottky diodes onto silicon using SU-8 for epitaxy transfer. In: 2018 IEEE/MTT-S international microwave symposium-IMS, pp 769–772
2. Jafari M, Moradi G, Shirazi RS, Mirzavand R (2017) Design and implementation of a six-port junction based on substrate integrated waveguide. Turk J Electr Eng Comput Sci 25:2547–2553
3. Nadri S, Xie L, Jafari M, Bauwens MF, Arsenovic A, Weikle RM (2019) Measurement and extraction of parasitic parameters of quasi-vertical schottky diodes at submillimeter wavelengths. IEEE Microw Wirel Compon Lett 29:474–476
4. Gao W, Dimitrov D, Abdo H (2018) Tight independent set neighborhood union condition for fractional critical deleted graphs and ID deleted graphs. Discret Contin Dyn Syst-S 12:711–721
5. Gao W, Guirao JLG, Basavanagoud B, Wu J (2018) Partial multi-dividing ontology learning algorithm. Inf Sci 467:35–58
6. Gao W, Wang W, Dimitrov D, Wang Y (2018) Nano properties analysis via fourth multiplicative ABC indicator calculating. Arab J Chem 11:793–801
7. Gao W, Wu H, Siddiqui MK, Baig AQ (2018) Study of biological networks using graph theory. Saudi J Biol Sci 25:1212–1219
8. Gao W, Guirao JLG, Abdel-Aty M, Xi W (2019) An independent set degree condition for fractional critical deleted graphs. Discret & Cont Dyn Syst-S 12:877–886
9. Qiao W, Yang Z, Kang Z, Pan Z (2020) Short-term natural gas consumption prediction based on Volterra adaptive filter and improved whale optimization algorithm. Eng Appl Artif Intell 87:103323
10. Qiao W, Yang Z (2019) Forecast the electricity price of US using a wavelet transform-based hybrid model. Energy 1:116704
11. Qiao W, Yang Z (2019) Solving large-scale function optimization problem by using a new metaheuristic algorithm based on quantum dolphin swarm algorithm. IEEE Access 7:138972–138989
12. Qiao W, Tian W, Tian Y, Yang Q, Wang Y, Zhang J (2019) The forecasting of PM 2.5 using a hybrid model based on wavelet transform and an improved deep learning algorithm. IEEE Access 7:142814–142825
13. Qiao W, Yang Z (2019) Modified dolphin swarm algorithm based on chaotic maps for solving high-dimensional function optimization problems. IEEE Access 7:110472–110486
14. Qiao W, Huang K, Azimi M, Han S (2019) A novel hybrid prediction model for hourly gas consumption in supply side based on improved machine learning algorithms. IEEE Access 7:88218
15. Abualnour M, Chikh A, Hebali H, Kaci A, Tounsi A, Bousahla AA et al (2019) Thermomechanical analysis of antisymmetric laminated reinforced composite plates using a new four variable trigonometric refined plate theory. Comput Concret 24:489–498
16. Draiche K, Bousahla AA, Tounsi A, Alwabli AS, Tounsi A, Mahmoud S (2019) Static analysis of laminated reinforced composite plates using a simple first-order shear deformation theory. Comput Concret 24:369–378
17. Belbachir N, Draich K, Bousahla AA, Bourada M, Tounsi A, Mohammadimehr M (2019) Bending analysis of anti-symmetric cross-ply laminated plates under nonlinear thermal and mechanical loadings. Steel Composit Struct 33:81–92
18. Sahla M, Saidi H, Draiche K, Bousahla AA, Bourada F, Tounsi A (2019) Free vibration analysis of angle-ply laminated composite and soft core sandwich plates. Steel Composit Struct 33:663
19. Tajziehchi K, Ghabussi A, Alizadeh H (2018) Control and optimization against earthquake by using genetic algorithm. J Appl Eng Sci 8:73–78
20. Safarpour H, Ghanizadeh SA, Habibi M (2018) Wave propagation characteristics of a cylindrical laminated composite nanoshell in thermal environment based on the nonlocal strain gradient theory. Eur Phys J Plus 133:532
21. Zeighampour H, Beni YT, Karimipour I (2017) Material length scale and nonlocal effects on the wave propagation of composite laminated cylindrical micro/nanoshells. Eur Phys J Plus 132:503
22. Sahmani S, Fattahi A, Ahmed N (2018) Analytical mathematical solution for vibrational response of postbuckled laminated

FG-GPLRC nonlocal strain gradient micro-/nanobeams. Eng Comput 1:1–17
23. Safaei B, Khoda FH, Fattahi A (2019) Non-classical plate model for single-layered graphene sheet for axial buckling. Adv Nano Res 7:265–275
24. Safaei B, Ahmed N, Fattahi A (2019) Free vibration analysis of polyethylene/CNT plates. Eur Phys J Plus 134:271
25. Alizadeh M, Fattahi A (2019) Non-classical plate model for FGMs. Eng Comput 35:215–228
26. Fattahi A, Sahmani S, Ahmed N (2019) Nonlocal strain gradient beam model for nonlinear secondary resonance analysis of functionally graded porous micro/nano-beams under periodic hard excitations. Mech Based Des Struct Mach 1:1–30
27. Sahmani S, Fattahi A, Ahmed N (2019) Size-dependent nonlinear forced oscillation of self-assembled nanotubules based on the nonlocal strain gradient beam model. J Brazil Soc Mech Sci Eng 41:239
28. Sahmani S, Fattahi A, Ahmed N (2019) Analytical treatment on the nonlocal strain gradient vibrational response of postbuckled functionally graded porous micro-/nanoplates reinforced with GPL. Eng Comput 1:1–20
29. Sahmani S, Fattahi A (2017) Thermo-electro-mechanical size-dependent postbuckling response of axially loaded piezoelectric shear deformable nanoshells via nonlocal elasticity theory. Microsyst Technol 23:5105–5119
30. Ghadiri M, Shafiei N, Safarpour H (2017) Influence of surface effects on vibration behavior of a rotary functionally graded nanobeam based on Eringen’s nonlocal elasticity. Microsyst Technol 23:1045–1065
31. Safarpour H, Mohammadi K, Ghadiri M, Barooti MM (2018) Effect of Porosity on Flexural Vibration of CNT-Reinforced Cylindrical Shells in Thermal Environment Using GDQM. Int J Struct Stabil Dyn 1:1850123
32. SafarPour H, Ghanbari B, Ghadiri M (2018) Buckling and free vibration analysis of high speed rotating carbon nanotube reinforced cylindrical piezoelectric shell. Appl Math Model 1:1
33. Shojaeefard M, Mahinzare M, Safarpour H, Googarchin HS, Ghadiri M (2018) Free vibration of an ultra-fast-rotating-induced cylindrical nano-shell resting on a Winkler foundation under thermo-electro-magneto-elastic condition. Appl Math Model 61:255–279
34. Dehkordi SF, Beni YT (2017) Electro-mechanical free vibration of single-walled piezoelectric/flexoelectric nano cones using consistent couple stress theory. Int J Mech Sci 128:125–139
35. Arefi M (2018) Analysis of a doubly curved piezoelectric nano shell: nonlocal electro-elastic bending solution. Eur J Mech-A/Solids 70:226–237
36. Razavi H, Babadi AF, Beni YT (2017) Free vibration analysis of functionally graded piezoelectric cylindrical nanoshell based on consistent couple stress theory. Compos Struct 160:1299–1309
37. Ninh DG, Bich DH (2018) Characteristics of nonlinear vibration of nanocomposite cylindrical shells with piezoelectric actuators under thermo-mechanical loads. Aerosp Sci Technol 77:595–609
38. Fang X-Q, Zhu C-S (2017) Size-dependent nonlinear vibration of nonhomogeneous shell embedded with a piezoelectric layer based on surface/interface theory. Compos Struct 160:1191–1197
39. Eftekhar H, Zeynali H, Nasihatgozar M (2018) Electro-magneto temperature-dependent vibration analysis of functionally graded-carbon nanotube-reinforced piezoelectric Mindlin cylindrical shells resting on a temperature-dependent, orthotropic elastic medium. Mech Adv Mater Struct 25:1–14
40. Vinyas M (2019) A higher-order free vibration analysis of carbon nanotube-reinforced magneto-electro-elastic plates using finite element methods. Compos B Eng 158:286–301
41. Zhu C-S, Fang X-Q, Liu J-X, Li H-Y (2017) Surface energy effect on nonlinear free vibration behavior of orthotropic piezoelectric cylindrical nano-shells. Eur J Mech-A/Solids 66:423–432
42. Singh VK, Panda SK (2017) Geometrical nonlinear free vibration analysis of laminated composite doubly curved shell panels embedded with piezoelectric layers. J Vib Control 23:2078–2093
43. Fan J, Huang J, Ding J, Zhang J (2017) Free vibration of functionally graded carbon nanotube-reinforced conical panels integrated with piezoelectric layers subjected to elastically restrained boundary conditions. Adv Mech Eng 9:1687814017711811
44. Ebrahimi F, Hashemabadi D, Habibi M, Safarpour H (2019) Thermal buckling and forced vibration characteristics of a porous GNP reinforced nanocomposite cylindrical shell. Microsyst Technol 1:1–13
45. Karami B, Janghorban M, Tounsi A (2019) Galerkin’s approach for buckling analysis of functionally graded anisotropic nanoplates/different boundary conditions. Eng Comput 35:1297–1316
46. Khosravi F, Hosseini SA, Tounsi A (2020) Torsional dynamic response of viscoelastic SWCNT subjected to linear and harmonic torques with general boundary conditions via Eringen’s nonlocal differential model. Eur Phys J Plus 135:183
47. Balubaid M, Tounsi A, Dakhel B, Mahmoud S (2019) Free vibration investigation of FG nanoscale plate using nonlocal two variables integral refined plate theory. Comput Concret 24:579–586
48. Hussain M, Naeem MN, Tounsi A, Taj M (2019) Nonlocal effect on the vibration of armchair and zigzag SWCNTs with bending rigidity. Adv Nano Res 7:431
49. Boutaleb S, Benrahou KH, Bakora A, Algarni A, Bousahla AA, Tounsi A et al (2019) Dynamic analysis of nanosize FG rectangular plates based on simple nonlocal quasi 3D HSDT. Adv Nano Res 7:191
50. Alimirzaei S, Mohammadimehr M, Tounsi A (2019) Nonlinear analysis of viscoelastic micro-composite beam with geometrical imperfection using FEM: mSGT electro-magneto-elastic bending, buckling and vibration solutions. Struct Eng Mech 71:485–502
51. Semmah A, Heireche H, Bousahla AA, Tounsi A (2019) Thermal buckling analysis of SWBNNT on Winkler foundation by non local FSDT. Adv Nano Res 7:89
52. Karami B, Janghorban M, Tounsi A (2020) Novel study on functionally graded anisotropic doubly curved nanoshells. Eur Phys J Plus 135:103
53. Tlidji Y, Zidour M, Draiche K, Safa A, Bourada M, Tounsi A et al (2019) Vibration analysis of different material distributions of functionally graded microbeam. Struct Eng Mech 69:637–649
54. Berghouti H, Adda Bedia E, Benkhedda A, Tounsi A (2019) Vibration analysis of nonlocal porous nanobeams made of functionally graded material. Advances in Nano Research 7:351–364
55. Bedia WA, Houari MSA, Bessaim A, Bousahla AA, Tounsi A, Saeed T et al (2019) A new hyperbolic two-unknown beam model for bending and buckling analysis of a nonlocal strain gradient nanobeams. J Nano Res 1:175–191
56. Karami B, Janghorban M, Tounsi A (2019) Wave propagation of functionally graded anisotropic nanoplates resting on Winkler–Pasternak foundation. Structural Engineering and Mechanics 70:55–66
57. Karami B, Shahsavari D, Janghorban M, Tounsi A (2019) Resonance behavior of functionally graded polymer composite nanoplates reinforced with graphene nanoplatelets. Int J Mech Sci 156:94–105
58. Karami B, Janghorban M, Tounsi A (2019) On exact wave propagation analysis of triclinic material using three-dimensional bi-Helmholtz gradient plate model. Struct Eng Mech 69:487–497
59. Karami B, Janghorban M, Tounsi A (2019) On pre-stressed functionally graded anisotropic nanoshell in magnetic field. J Brazil Soc Mech Sci Eng 41:495
60. Ghabussi A, Marnani JA, Rohanimanesh MS (2020) Improving seismic performance of portal frame structures with steel curved dampers. Structures 1:27–40

61. Wang Z-W, Han Q-F, Nash DH, Liu P-Q (2017) Investigation on inconsistency of theoretical solution of thermal buckling critical temperature rise for cylindrical shell. Thin-Walled Struct 119:438–446
62. Safarpour H, Hajilak ZE, Habibi M (2019) A size-dependent exact theory for thermal buckling, free and forced vibration analysis of temperature dependent FG multilayer GPLRC composite nanostructures restring on elastic foundation. International Journal of Mechanics and Materials in Design 15:1–15
63. Kaddari M, Kaci A, Bousahla AA, Tounsi A, Bourada F, Bedia EA et al (2020) A study on the structural behaviour of functionally graded porous plates on elastic foundation using a new quasi-3D model: bending and free vibration analysis. Comput Concret 25:37
64. Addou FY, Meradjah M, Bousahla AA, Benachour A, Bourada F, Tounsi A et al (2019) Influences of porosity on dynamic response of FG plates resting on Winkler/Pasternak/Kerr foundation using quasi 3D HSDT. Comput Concret 24:347–367
65. Khiloun M, Bousahla AA, Kaci A, Bessaim A, Tounsi A, Mahmoud S (2019) Analytical modeling of bending and vibration of thick advanced composite plates using a four-variable quasi 3D HSDT. Eng Comput 1:1–15
66. Zarga D, Tounsi A, Bousahla AA, Bourada F, Mahmoud S (2019) Thermomechanical bending study for functionally graded sandwich plates using a simple quasi-3D shear deformation theory. Steel Compos Struct 32:389–410
67. Boulefrakh L, Hebali H, Chikh A, Bousahla AA, Tounsi A, Mahmoud S (2019) The effect of parameters of visco-Pasternak foundation on the bending and vibration properties of a thick FG plate. Geomech Eng 18:161–178
68. Boukhlif Z, Bouremana M, Bourada F, Bousahla AA, Bourada M, Tounsi A et al (2019) A simple quasi-3D HSDT for the dynamics analysis of FG thick plate on elastic foundation. Steel Compos Struct 31:503–516
69. Mahmoudi A, Benyoucef S, Tounsi A, Benachour A, Adda Bedia EA, Mahmoud S (2019) A refined quasi-3D shear deformation theory for thermo-mechanical behavior of functionally graded sandwich plates on elastic foundations. Journal of Sandwich Structures & Materials 21:1906–1929
70. Zaoui FZ, Ouinas D, Tounsi A (2019) New 2D and quasi-3D shear deformation theories for free vibration of functionally graded plates on elastic foundations. Compos B Eng 159:231–247
71. Safarpour H, Barooti M, Ghadiri M (2019) Influence of rotation on vibration behavior of a functionally graded moderately thick cylindrical nanoshell considering initial hoop tension. J Solid Mech 11:254–271
72. Ebrahimi F, Safarpour H (2018) Vibration analysis of inhomogeneous nonlocal beams via a modified couple stress theory incorporating surface effects. Wind Struct 27:431–438
73. Mohammadi K, Barouti MM, Safarpour H, Ghadiri M (2019) Effect of distributed axial loading on dynamic stability and buckling analysis of a viscoelastic DWCNT conveying viscous fluid flow. J Brazil Soc Mech Sci Eng 41:93
74. SafarPour H, Hosseini M, Ghadiri M (2017) Influence of three-parameter viscoelastic medium on vibration behavior of a cylindrical nonhomogeneous microshell in thermal environment: an exact solution. J Therm Stresses 40:1353–1367
75. Safarpour H, Mohammadi K, Ghadiri M, Barooti MM (2018) Effect of porosity on flexural vibration of CNT-reinforced cylindrical shells in thermal environment using GDQM. Int J Struct Stab Dyn 18:1850123
76. Safarpour H, Mohammadi K, Ghadiri M (2017) Temperature-dependent vibration analysis of a FG viscoelastic cylindrical microshell under various thermal distribution via modified length scale parameter: a numerical solution. J Mech Behav Mater 26:9–24
77. SafarPour H, Ghanbari B, Ghadiri M (2019) Buckling and free vibration analysis of high speed rotating carbon nanotube reinforced cylindrical piezoelectric shell. Appl Math Model 65:428–442
78. Ghadiri M, Safarpour H (2016) Free vibration analysis of embedded magneto-electro-thermo-elastic cylindrical nanoshell based on the modified couple stress theory. Appl Phys A 122:833
79. Ghadiri M, SafarPour H (2017) Free vibration analysis of size-dependent functionally graded porous cylindrical microshells in thermal environment. J Therm Stresses 40:55–71
80. SafarPour H, Ghadiri M (2017) Critical rotational speed, critical velocity of fluid flow and free vibration analysis of a spinning SWCNT conveying viscous fluid. Microfluid Nanofluid 21:22
81. Barooti MM, Safarpour H, Ghadiri M (2017) Critical speed and free vibration analysis of spinning 3D single-walled carbon nanotubes resting on elastic foundations. Eur Phys J Plus 132:6
82. SafarPour H, Mohammadi K, Ghadiri M, Rajabpour A (2017) Influence of various temperature distributions on critical speed and vibrational characteristics of rotating cylindrical microshells with modified lengthscale parameter. Eur Phys J Plus 132:281
83. Ebrahimi F, Habibi M, Safarpour H (2018) On modeling of wave propagation in a thermally affected GNP-reinforced imperfect nanocomposite shell. Eng Comput 1:1–15
84. Reddy JN (2004) Mechanics of laminated composite plates and shells: theory and analysis. CRC Press, Boca Raton
85. Medani M, Benahmed A, Zidour M, Heireche H, Tounsi A, Bousahla AA et al (2019) Static and dynamic behavior of (FG-CNT) reinforced porous sandwich plate using energy principle. Steel Compos Struct 32:595–610
86. Boussoula A, Boucham B, Bourada M, Bourada F, Tounsi A, Bousahla A et al (2019) A simple nth-order shear deformation theory for thermomechanical bending analysis of different configurations of FG sandwich plates. Smart Struct Syst (Accepted)
87. Chaabane LA, Bourada F, Sekkal M, Zerouati S, Zaoui FZ, Tounsi A et al (2019) Analytical study of bending and free vibration responses of functionally graded beams resting on elastic foundation. Struct Eng Mech 71:185–196
88. Bourada F, Bousahla AA, Bourada M, Azzaz A, Zinata A, Tounsi A (2019) Dynamic investigation of porous functionally graded beam using a sinusoidal shear deformation theory. Wind Struct 28:19–30
89. Draoui A, Zidour M, Tounsi A, Adim B (2019) Static and dynamic behavior of nanotubes-reinforced sandwich plates using (FSDT). J Nano Res 1:117–135
90. Meksi R, Benyoucef S, Mahmoudi A, Tounsi A, Adda Bedia EA, Mahmoud S (2019) An analytical solution for bending, buckling and vibration responses of FGM sandwich plates. Journal of Sandwich Structures & Materials 21:727–757
91. Hellal H, Bourada M, Hebali H, Bourada F, Tounsi A, Bousahla AA et al (2019) Dynamic and stability analysis of functionally graded material sandwich plates in hygro-thermal environment using a simple higher shear deformation theory. J Sandw Struct Mater. https://doi.org/10.1177/1099636219845841
92. Safarpour M, Ghabussi A, Ebrahimi F, Habibi M, Safarpour H (2020) Frequency characteristics of FG-GPLRC viscoelastic thick annular plate with the aid of GDQM. Thin-Walled Struct 150:106683
93. Safarpour M, Ebrahimi F, Habibi M, Safarpour H (2020) On the nonlinear dynamics of a multi-scale hybrid nanocomposite disk. Eng Comput 1(1–20):2020
94. Moayedi H, Habibi M, Safarpour H, Safarpour M, Foong L (2019) Buckling and frequency responses of a graphen nanoplatelet reinforced composite microdisk. Int J Appl Mech 11:1950102
95. Moayedi H, Darabi R, Ghabussi A, Habibi M, Foong LK (2020) Weld orientation effects on the formability of tailor welded thin steel sheets. Thin-Walled Struct 149:106669

96. Ghazanfari A, Soleimani SS, Keshavarzzadeh M, Habibi M, Assempuor A, Hashemi R (2019) Prediction of FLD for sheet metal by considering through-thickness shear stresses. Mech Based Des Struct Mach 1:1–18
97. Alipour M, Torabi MA, Sareban M, Lashini H, Sadeghi E, Fazaeli A et al (2019) Finite element and experimental method for analyzing the effects of martensite morphologies on the formability of DP steels. Mech Based Des Struct Mach 1:1–17
98. Hosseini S, Habibi M, Assempour A (2018) Experimental and numerical determination of forming limit diagram of steel-copper two-layer sheet considering the interface between the layers. Modar Mech Eng 18:174–181
99. Habibi M, Hashemi R, Ghazanfari A, Naghdabadi R, Assempour A (2018) Forming limit diagrams by including the M-K model in finite element simulation considering the effect of bending. Proc Inst Mech Eng Part L: J Mater Des Appl 232:625–636
100. Habibi M, Payganeh G (2018) Experimental and finite element investigation of titanium tubes hot gas forming and production of square cross-section specimens
101. Habibi M, Hashemi R, Tafti MF, Assempour A (2018) Experimental investigation of mechanical properties, formability and forming limit diagrams for tailor-welded blanks produced by friction stir welding. J Manuf Process 31:310–323
102. Habibi M, Ghazanfari A, Assempour A, Naghdabadi R, Hashemi R (2017) Determination of forming limit diagram using two modified finite element models. Mech Eng 48:141–144
103. Ghazanfari A, Assempour A, Habibi M, Hashemi R (2016) Investigation on the effective range of the through thickness shear stress on forming limit diagram using a modified Marciniak–Kuczynski model. Modar Mech Eng 16:137–143
104. Habibi M, Hashemi R, Sadeghi E, Fazaeli A, Ghazanfari A, Lashini H (2016) Enhancing the mechanical properties and formability of low carbon steel with dual-phase microstructures. J Mater Eng Perform 25:382–389
105. Fazaeli A, Habibi M, Ekrami A (2016) Experimental and finite element comparison of mechanical properties and formability of dual phase steel and ferrite-pearlite steel with the same chemical composition. Metall Eng 19(2):84–93
106. Tsai S (2018) Introduction to composite materials. Routledge, London
107. Shokrgozar A, Ghabussi A, Ebrahimi F, Habibi M, Safarpour H (2020) Viscoelastic dynamics and static responses of a graphene nanoplatelets-reinforced composite cylindrical microshell. Mech Based Des Struct Mach 1:1–28
108. lori ES, Ebrahimi F, Supeni EEB et al (2020) Frequency characteristics of a GPL-reinforced composite microdisk coupled with a piezoelectric layer. Eur Phys J Plus 135:144. https://doi.org/10.1140/epjp/s13360-020-00217-x
109. Moayedi H, Aliakbarlou H, Jebeli M, Noormohammadi Arani O, Habibi M, Safarpour H et al (2019) Thermal buckling responses of a graphene reinforced composite micropanel structure. Int J Appl Mech 1:1. https://doi.org/10.1142/S1758825120500106
110. Shokrgozar A, Safarpour H, Habibi M (2020) Influence of system parameters on buckling and frequency analysis of a spinning cantilever cylindrical 3D shell coupled with piezoelectric actuator. Proc Inst Mech Eng Part C J Mech Eng Sci 234:512–529
111. Ghabussi A, Ashrafi N, Shavalipour A, Hosseinpour A, Habibi M, Moayedi H et al (2019) Free vibration analysis of an electro-elastic GPLRC cylindrical shell surrounded by viscoelastic foundation using modified length-couple stress parameter. Mech Based Des Struct Mach 1:1–25
112. Habibi M, Mohammadi A, Safarpour H, Ghadiri M (2019) Effect of porosity on buckling and vibrational characteristics of the imperfect GPLRC composite nanoshell. Mech Based Des Struct Mach 1(1–30):2019
113. Habibi M, Mohammadi A, Safarpour H, Shavalipour A, Ghadiri M (2019) Wave propagation analysis of the laminated cylindrical nanoshell coupled with a piezoelectric actuator. Mechanics Based Design of Structures and Machines 1:1–19
114. Ebrahimi F, Mohammadi K, Barouti MM, Habibi M (2019) Wave propagation analysis of a spinning porous graphene nanoplatelet-reinforced nanoshell. Waves Random Complex Med 1:1–27
115. Habibi M, Taghdir A, Safarpour H (2019) Stability analysis of an electrically cylindrical nanoshell reinforced with graphene nanoplatelets. Compos B Eng 175:107125
116. Mohammadgholiha M, Shokrgozar A, Habibi M, Safarpour H (2019) Buckling and frequency analysis of the nonlocal strain–stress gradient shell reinforced with graphene nanoplatelets. J Vib Control 25:2627–2640
117. Ebrahimi F, Habibi M, Safarpour H (2019) On modeling of wave propagation in a thermally affected GNP-reinforced imperfect nanocomposite shell. Eng Comput 35:1375–1389
118. Safarpour H, Hajilak ZE, Habibi M (2019) A size-dependent exact theory for thermal buckling, free and forced vibration analysis of temperature dependent FG multilayer GPLRC composite nanostructures restring on elastic foundation. Int J Mech Mater Des 15:569–583
119. Hashemi HR, Alizadeh AA, Oyarhossein MA, Shavalipour A, Makkiabadi M, Habibi M (2019) Influence of imperfection on amplitude and resonance frequency of a reinforcement compositionally graded nanostructure. Waves Random Complex Med 1(1–27):2019
120. EsmailpoorHajilak Z, Pourghader J, Hashemabadi D, Sharifi Bagh F, Habibi M, Safarpour H (2019) Multilayer GPLRC composite cylindrical nanoshell using modified strain gradient theory. Mech Based Des Struct Mach 47:521–545
121. Ebrahimi F, Hajilak ZE, Habibi M, Safarpour H (2019) Buckling and vibration characteristics of a carbon nanotube-reinforced spinning cantilever cylindrical 3D shell conveying viscous fluid flow and carrying spring-mass systems under various temperature distributions. Proc Inst Mech Eng Part C J Mech Eng Sci 233:4590–4605
122. Mohammadi A, Lashini H, Habibi M, Safarpour H (2019) Influence of viscoelastic foundation on dynamic behaviour of the double walled cylindrical inhomogeneous micro shell using MCST and with the aid of GDQM. J Solid Mech 11:440–453
123. Habibi M, Hashemabadi D, Safarpour H (2019) Vibration analysis of a high-speed rotating GPLRC nanostructure coupled with a piezoelectric actuator. Eur Phys J Plus 134:307
124. Pourjabari A, Hajilak ZE, Mohammadi A, Habibi M, Safarpour H (2019) Effect of porosity on free and forced vibration characteristics of the GPL reinforcement composite nanostructures. Comput Math Appl 77:2608–2626
125. Habibi M, Mohammadgholiha M, Safarpour H (2019) Wave propagation characteristics of the electrically GNP-reinforced nanocomposite cylindrical shell. J Braz Soc Mech Sci Eng 41:221
126. Safarpour H, Pourghader J, Habibi M (2019) Influence of spring-mass systems on frequency behavior and critical voltage of a high-speed rotating cantilever cylindrical three-dimensional shell coupled with piezoelectric actuator. J Vib Control 25:1543–1557
127. Asl MH, Farivar B, Momenzadeh S (2019) Investigation of the rigidity of welded shear tab connections. Eng Struct 179:353–366
128. Tadi Beni Y, Mehralian F, Zeighampour H (2016) The modified couple stress functionally graded cylindrical thin shell formulation. Mech Adv Mater Struct 23:791–801